ACS central science

Research Article

http://pubs.acs.org/journal/acscii

Assessing Physicochemical Properties of Drug Molecules via Microsolvation Measurements with Differential Mobility Spectrometry

Chang Liu,[†] J. C. Yves Le Blanc,[†] Bradley B. Schneider,[†] Jefry Shields,[‡] James J. Federico, III,[‡] Hui Zhang,[‡] Justin G. Stroh,[‡] Gregory W. Kauffman,[‡] Daniel W. Kung,[‡] Christian Ieritano,[§] Evan Shepherdson,[§] Mitch Verbuyst,[§] Luke Melo,[§] Moaraj Hasan,[§] Dalia Naser,[§] John S. Janiszewski,*[,‡] W. Scott Hopkins,*[,§] and J. Larry Campbell*[,†,§]

[†]SCIEX, 71 Four Valley Drive, Concord, Ontario, L4K 4V8, Canada

[‡]Pfizer Global Research and Development, Eastern Point Road, Groton, Connecticut 06340, United States

[§]Department of Chemistry, University of Waterloo, 200 University Avenue West, Waterloo, Ontario, N2L 3G1, Canada

Supporting Information

ABSTRACT: The microsolvated state of a molecule, represented by its interactions with only a small number of solvent molecules, can play a key role in determining the observable bulk properties of the molecule. This is especially true in cases where strong local hydrogen bonding exists between the molecule and the solvent. One method that can probe the microsolvated states of charged molecules is differential mobility spectrometry (DMS), which rapidly interrogates an ion's transitions between a solvated and desolvated state in the gas phase (i.e., few solvent molecules present). However, can the results of DMS analyses of a class of molecules reveal information about the bulk physicochemical properties of those species? Our findings presented here show that DMS behaviors correlate strongly with the measured solution phase pK_a and pK_b values, and cell permeabilities of a set of structurally related drug molecules, even yielding high-resolution discrimination between isomeric forms of these drugs. This is due to DMS's ability to separate species based upon only subtle (yet predictable) changes in structure: the same subtle changes that can influence isomers' different bulk properties. Using 2-methylquinolin-8-ol as the core structure, we demonstrate how DMS shows promise for rapidly and sensitively probing the physicochemical properties of molecules, with particular attention paid to drug candidates at the early stage of drug development. This study serves as a foundation upon which future drug molecules of different structural classes could be examined.

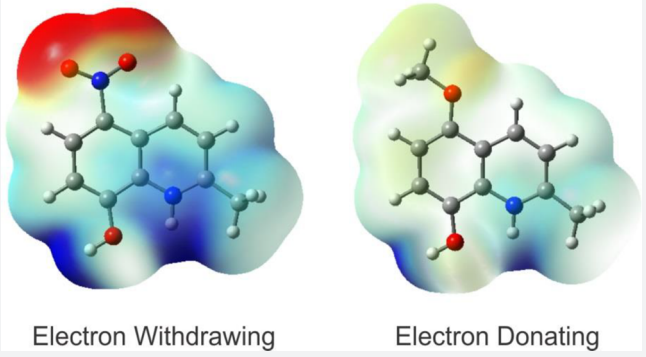

INTRODUCTION

Many studies involving microsolvated species—isolated ions or molecules bound noncovalently to a small, defined number of solvent molecules—usually reflect on whether the knowledge gained provides valuable insights into their analogous bulk-solvated states.[1] That is, do the properties of microsolvated species teach us anything about the same molecules' behavior as observed in liquid solution? Ultimately, it is the presence of any strong correlations observed between the properties of microsolvated molecules and their bulk-solvated forms and a reasonably argued theory explaining these relationships that lend the best support to such comparisons.

Among the many analytical tools employed to study the microsolvated states of molecules is differential mobility spectrometry (DMS).[2−4] While DMS is a technology known more for its ability to separate analytical ions from chemical noise,[5] we have recently employed DMS to examine how the microsolvation properties of ions are affected by their specific structural attributes. For example, we have observed the influence of electronic/resonance effects,[6] the steric hindrance of charge sites,[7−9] and the influence of intramolecular hydrogen bonding on DMS behavior.[10] Based upon these recent discoveries, we focused efforts on determining whether any links could be made between the DMS-probed microsolvation of molecules and their bulk physicochemical properties.

Medicinal chemistry, more specifically drug design, might benefit from a technology such as DMS that could help predict molecular physicochemical properties with sensitivity and speed. Presently, during the early stages of small molecule drug discovery, medicinal chemists try to relate a drug candidate's chemical structure and physicochemical properties

Received: October 5, 2016
Published: February 10, 2017

DOI: 10.1021/acscentsci.6b00297
ACS Cent. Sci. 2017, 3, 101−109

to its cellular availability.[11,12] Many of these properties can be experimentally measured using cell-based permeability assays (e.g., MDCK, RRCK, Caco-2),[13] and physicochemical examination (e.g., pK_a, shake-flask log D, PAMPA, turbidometry).[14] These benchtop *in vitro* studies serve as preliminary appraisals of a molecule's fitness to navigate biological barriers *in vivo*. Unfortunately, existing methodologies lack the resolution to discriminate between closely related structural analogues or motifs.[15,16] Moreover, while progress has been made in streamlining these assays,[17−19] they still require considerable resources and experience suboptimal reproducibility.[20,21]

With this as our focus, we report on the use of DMS as a probe of the microsolvated forms of drug molecules, and relate the measured DMS behavior to those drug molecules' condensed phase physicochemical properties. Here, we demonstrate that the DMS properties of drug molecules, which measure the molecule's binding interactions with a protic solvent vapor, correlate strongly with experimentally determined pK_a, pK_b, and cell permeability measurements. Moreover, these measurements require only a fraction of the time, sample, and resources of current state-of-the-art techniques (*vide infra*). These correlations derive from the ability of the DMS instrument to probe the ion−solvent interactions of gas-phase forms of drug molecules, which relates to both a drug molecule's inherent acidity/basicity (pK_a/pK_b) and its ability to desolvate such that it might transit a hydrophobic lipid bilayer (cell permeability). Our findings demonstrate that, in addition to being able to distinguish isomeric drug molecules easily, the DMS behaviors of drug molecules can be predicted based upon subtle changes in structure related back to specific Hammett parameters (σ^+) and van der Waals radii of the functional groups.

RESULTS AND DISCUSSION

The DMS Behaviors of Drug Molecules Correlate Strongly with Their Passive Cell Permeabilities. In this study, we employed DMS−MS to examine drug molecules that shared a common core: 2-methylquinolin-8-ol (Scheme 1).

Scheme 1. Structures of the 2-Methylquinolin-8-ol Molecules Analyzed in This Study (22 in Total)

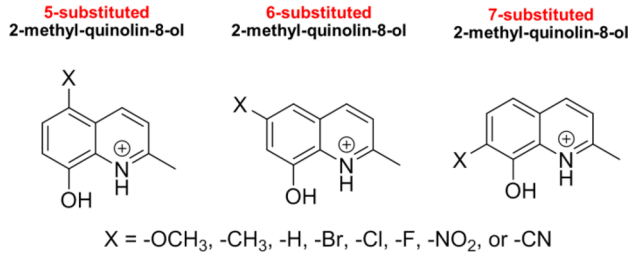

This drug and its analogues have been employed for years in a variety of pharmaceutical applications and physicochemical studies.[22−32] In total, we examined 22 drug molecules: 7 triplets of isomers (each bearing one of 7 functional groups in either the 5-, 6-, or 7-position of the quinoline ring) as well as 2-methylquinolin-8-ol itself. One of the reasons for choosing this model drug chemistry was that several types of structural motifs are present that could impact the microsolvation, as well as the bulk physicochemical properties of these molecules; the different functional groups provide opportunities for varied steric and electronic effects to be present, as well as the presence of intramolecular hydrogen bonds (IMHBs), that could also impact the behavior of these molecules. Overall, our aim was to relate the DMS-based ion−solvent interaction measurements to *in vitro* diagnostics of interest to medicinal chemists, including the passive cell permeability using the Ralph-Russ Canine Kidney (RRCK) method[33] and experimentally determined pK_a/pK_b measurements.[19,34] These conventional methodologies are described in more detail in the Supporting Information.

The critical DMS output that relates directly to a specific molecule's solvent binding energy is the relationship between the applied separation voltage (SV) and the measured optimum compensation voltage (CV) for transmission of the ionized drugs through the DMS cell (see Supporting Information for further detail).[9] For example, Figure 1 depicts the results of the

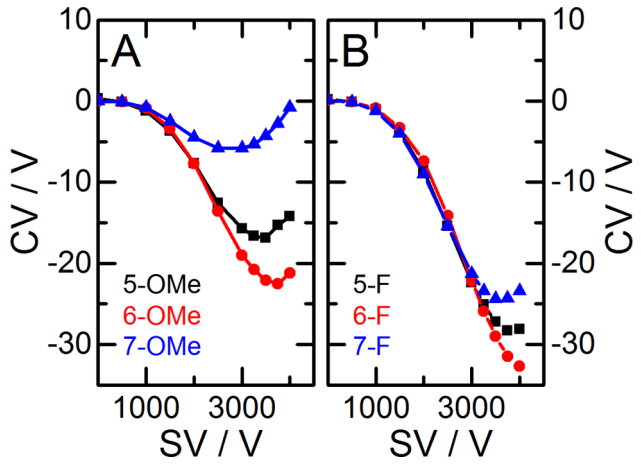

Figure 1. DMS dispersion plots (A) methoxy-2-methylquinolin-8-ol and (B) fluoro-2-methylquinolin-8-ol in a N_2 environment seeded with 1.5% methanol vapor. Substitution occurs at the 5- (black squares), 6- (red circles), and 7-positions (blue triangles).

DMS CV-ramping experiments conducted with three isomers of methoxy-2-methylquinolin-8-ol and fluoro-2-methylquinolin-8-ol where SV was stepped from 0 to 4000 V. There are clear trends for each drug as the site of substitution is varied from the 5-, to 6-, to 7-positions (see Scheme 1).

The more negative the CV shift experienced by the protonated drug molecule, the stronger the interaction with the solvent vapor that molecule exhibits.[7,9] Thus, for both the methoxy- and fluoro-substituted drugs, the 7-substituted isomer displayed the weakest ion−solvent interaction, followed by the 5- and then the 6-substituted isomers. Moreover, the overall magnitude of the negative CV shifts was greater for the fluoro-substituted drugs than for the methoxy-substituted species, revealing the greater ion−solvent interactions of the fluoro-substituted molecules (*vide infra*). Similar DMS-based examinations were conducted for all 22 drug molecules. Ultimately, we have found that the SV value at which at ion's CV reaches a minimum value (SV@CV_{min}) represents a measure for the ion's desolvated/solvated equilibrium,[2,3,7,35] and overall, its ion−solvent binding (i.e., microsolvation) energy.[9]

Our comparison of the DMS data with the experimental physicochemical data yielded strong and promising correlations. Figure 2 plots cell permeability values and SV@CV_{min} measurements for three sets of structural isomers: methoxy-, chloro-, and cyano-2-methylquinolin-8-ol derivatives. It is clear that SV@CV_{min} measurements track with the relative cell

DOI: 10.1021/acscentsci.6b00297
ACS Cent. Sci. 2017, 3, 101−109

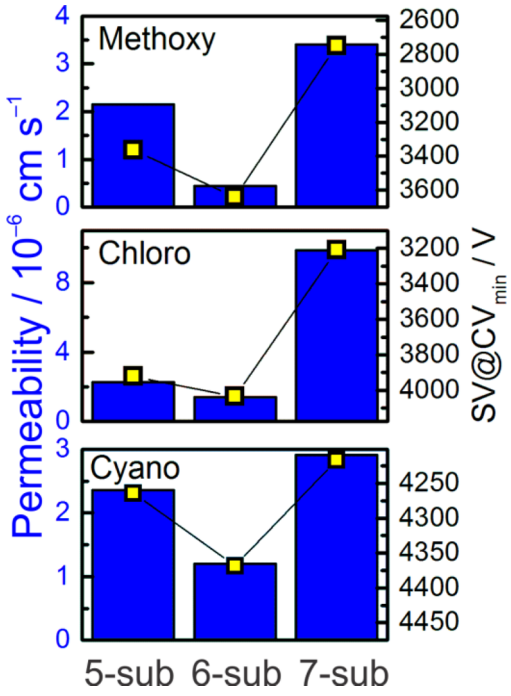

Figure 2. Plots showing the correlation between RRCK-based cell permeabilities (blue bar graphs) and SV@CV$_{min}$ (yellow data points) as a function of substitution position for the (top) methoxy-, (middle) chloro-, and (bottom) cyano-substituted 2-methylquinolin-8-ol derivatives.

permeability for each isomer of a given substituent. The subtle structural differences between these drug isomers can affect their respective solvent binding energies, resulting in the drugs' distinct relative cell permeabilities. For example, the more strongly microsolvated 6-substituted 2-quinolin-8-ol derivatives (i.e., those with larger SV@CV$_{min}$ values) display lower cellular permeability than the 5- and 7-substituted species. This result supports our hypothesis that stronger ion−solvent interactions correlate with slower desolvation and transport kinetics at the cell membrane, thereby lowering the rate of passive diffusion. Similar comparisons for all seven substituent groups are presented in Figure S1. The relationship between the observed DMS ion−solvent interaction and relative passive cell permeability is in accord with the general thinking behind the mechanism of passive transport of drug molecules across cell membranes.[36−39] As a drug molecule exhibits a greater tendency to shed solvent molecules from its immediate environment, it can then begin to interact with a cell's outer wall and proceed to transit this barrier.

In general, cell permeability is significantly higher for all 7-substituted isomers compared with their 5- and 6-substituted analogues. While this trend was consistent across the 2-methylquinolin-8-ol isomers for a particular substituent (Figure 2), the ion−solvent interactions of the different substituted derivatives (e.g., methoxy versus cyano) were not directly correlated with apparent cell permeability. For example, 7-methoxy-2-methylquinolin-8-ol and 7-cyano-2-methylquinolin-8-ol both exhibited a cell permeability of ∼3 × 10^{-6} cm s^{-1}, but the SV@CV$_{min}$ value for the 7-cyano derivative was significantly larger than that for the 7-methoxy analogue. Based on our hypothesis, we would expect greater cell permeability for the 7-methoxy analogue than for the 7-cyano species due to the weaker microsolvation of the methoxy species (i.e., lower values of SV@CV$_{min}$). These differences are presently under investigation.

The DMS Behaviors of Drug Molecules Also Correlate Strongly to pK_a and pK_b Measurements. The experimentally measured pK_a and pK_b values for the 2-methylquinolin-8-ol derivatives also correlate strongly with the DMS results. We observe that species with lower pK_a and pK_b values exhibit greater ion−solvent interactions (see Figures 3A and 3B); the 5- and 6-substituted 2-methylquinolin-8-ol

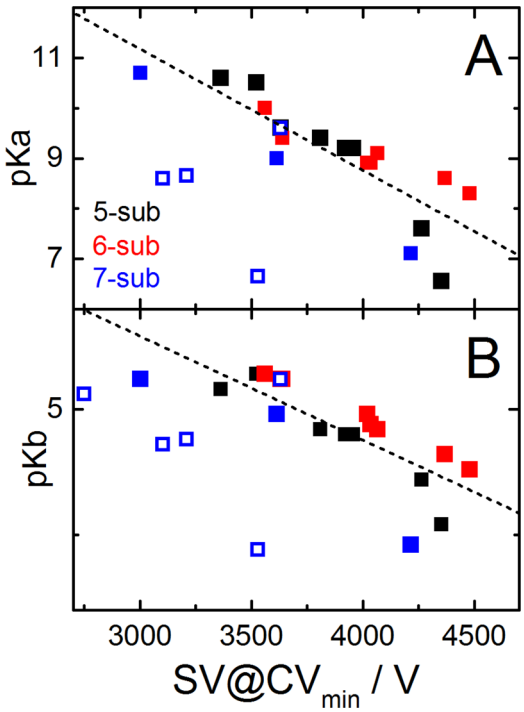

Figure 3. Experimentally determined (A) pK_a (R^2 = 0.70), and (B) pK_b (R^2 = 0.62), as a function of SV@CV$_{min}$ for 2-methylquinolin-8-ol derivatives: (black) 5-substituted, (red) 6-substituted, and (blue) 7-substituted species. Filled squares are species that bind to solvent via the OH group, while hollow blue squares are species that exhibit NH−solvent binding.

derivatives show strong correlations, but the 7-substituted isomers exhibit greater variability in this relationship (Figure 3, blue squares). We attribute this variability in the pK_a/pK_b−DMS correlation plots for the 7-substituted species to the variability in chemical and physical interactions between 7-position substituents and solvent molecules (afforded by the closer proximity to the solvent binding site). Indeed, we find that the data points which are furthest from the pK_a/pK_b−DMS correlation trend line are all associated with 7-substituted species that exhibit NH−solvent binding, rather than the more common OH solvent binding motif (hollow blue squares in Figure 3). In other words, the variability in the physicochemical properties of the 7-substituted derivatives arises due to steric effects, which in turn influence the solvent binding motif. The strong correlations that we observe for the 5- and 6-substituted species, on the other hand, demonstrate that DMS ion−solvent clustering measurements are sensitive to steric and electronic effects (*vide infra*).

Rationalizing the Correlations between DMS Behaviors and Physicochemical Properties. The ability for the DMS to measure SV@CV$_{min}$ values for a large collection of

DOI: 10.1021/acscentsci.6b00297
ACS Cent. Sci. 2017, 3, 101−109

drug molecules both rapidly (~2 min per analysis) and with great sensitivity (only picograms of material are required) makes the observed correlations between the DMS data and the physicochemical parameters very compelling. But what is the nature of the underlying mechanisms that link these gas-phase measurements with the mated *in vitro* experiments?

First, we must examine the other parameters with which DMS displays strong correlations: calculated ion−solvent binding energies (i.e., microsolvation energies) and functional group-specific linear free energy parameters (e.g., σ^+ values). The correlation between the DMS results and the calculated solvent binding energies for the twenty two 2-methylquinolin-8-ol species support a hypothesis that steric and electronic effects account for the observed variations in CVs. In addition, the fact that the binding energy for a single solvent molecule correlates best with the DMS data also supports a mechanism wherein a strong local hydrogen bond is playing a key role.[40]

Figures 4A and 4B plot the calculated methanol binding energies against measured DMS SV@CV_{min} for the 5- and 6-substituted 2-methylquinolin-8-ol species, respectively. Clearly, species which bind solvent molecules more strongly exhibit greater SV@CV_{min} values as measured by DMS. Figure 4C displays the correlation between binding energy and measured CV for the 7-substituted species. In this case, the voltages required to correct the ion trajectories encompass a much broader range and the correlation with calculated binding energies is poorer. As was the case with the pK_a/pK_b correlations (*vide supra*), the relatively poor correlation between calculated solvent binding energy and DMS ion trajectory for the 7-substituted species arises due to steric effects, which ultimately influence whether the solvent molecule is bound to the OH group or to the NH group. The data points for the 7-substituted species that favor the NH−solvent binding motif are plotted as hollow squares in Figure 4C. In general, the NH-bound solvent clusters exhibit weaker calculated binding energies and DMS-measured microsolvation energies than the species which favor the OH−solvent binding motif. Given the fact that across the series of 7-substituted derivatives we are probing two different ion−solvent binding motifs, each of which will exhibit inherently different clustering/declustering dynamics, it is not unreasonable to expect a higher degree of variability in the correlation plot.

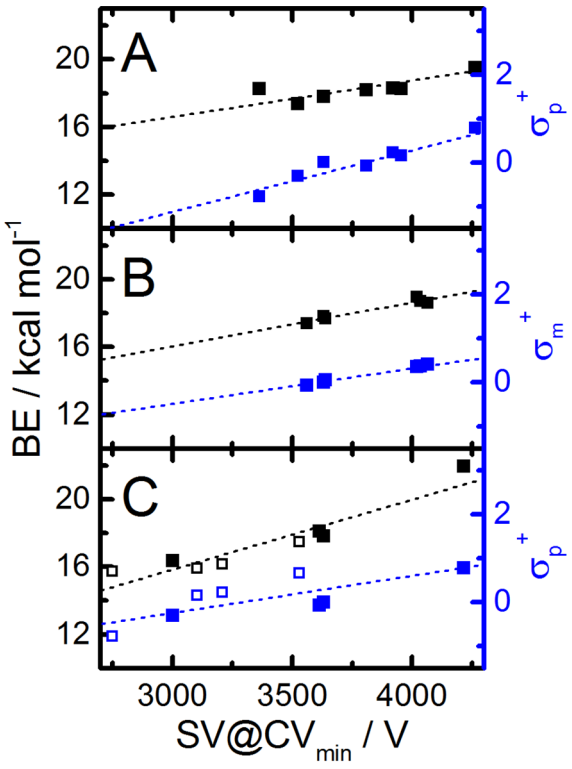

Figure 4. Plots displaying the correlations between the observed SV@CV_{min} measurements, calculated methanol binding energies, and sigma parameters (σ_p^+ for 5- and 7-substitution; σ_M^+ for 6-substitution) for the (A) 5-substituted (R^2_{BE} = 0.67; R^2_s = 0.91), (B) 6-substituted (R^2_{BE} = 0.97; R^2_σ = 0.99), and (C) 7-substituted (R^2_{BE} = 0.86; R^2_σ = 0.54) 2-methylquinolin-8-ol derivatives.

Also plotted in Figure 4 are the substituent-specific DMS behaviors of the electron-donating (ED) and electron-withdrawing (EW) groups, which are apparent for the 5-subsituted species through strong correlations with Brown and Okamoto's σ_p^+ constants (i.e., Hammett parameters; Table S1).[41,42] Similarly, the DMS behavior of the 6-substituted species trends consistently with the meta-position electrophilic substituent constants (σ_M^+, Table S1). However, as was the case with calculated solvent binding energies, the 7-substituted species exhibit a comparatively weaker correlation when plotting σ_p^+ versus measured SV@CV_{min}. Again, we attribute this to the convolution of resonance and steric effects for substituents at the 7-position,[23,24] a conclusion that we base on the fact that the species which exhibit NH−solvent binding (Figure 4C, hollow blue squares) seem to follow a slightly different trend than those which exhibit OH−solvent binding (Figure 4C, filled blue squares). Note also that substituents in the 7-position can potentially influence the microsolvation process via formation of an intramolecular hydrogen bond (IMHB) with the proton of the 8-hydroxy group (e.g., 7-nitro; see Supporting Information).[43] This notion is supported by the fact that, when the data for the 7-nitro substituted drugs are removed from the linear regression model of the DMS data comparison with cell permeability, pK_a, or pK_b (Figure S2, Table S3), the correlation improves. Further support for this conclusion comes from the calculated lowest-energy cluster geometries; many of the 7-substituted 2-methylquinolin-8-ol derivatives exhibit structures that suggest the possibility of intramolecular hydrogen bonding (see Supporting Information).[9] Moreover, our findings here are supported by past studies where the effects of electron-donating and electron-withdrawing substituents (and their respective σ or σ^+ constants) on pK_a[23,24,26,29] and solubility[30,32] have been examined for quinoline-8-ol derivatives. Ultimately, this apparent influence of electronic effects on DMS separation suggests a connection to linear free energy relationship and possibly to quantitative structure−activity relationships (QSAR).[44,45]

The behavior of the 7-substituted 2-methylquinolin-8-ol derivatives is similar to that of the 5-substituted isomers by virtue of the analogous electronic effects (i.e., charge delocalization) present (Scheme 2). However, the 7-substituted species induce a weaker ion−solvent binding interaction due to steric hindrance arising from the proximity of the functional group to the site of solvent binding. For all 5- and 6-substituted derivatives, solvent molecules were calculated to bind to the 8-hydroxy group in the lowest energy structures (see Supporting Information). However, as mentioned above, in some cases the global minima for the 7-substituted ion−solvent clusters exhibited NH-bound solvent molecules. Interestingly, this

DOI: 10.1021/acscentsci.6b00297
ACS Cent. Sci. 2017, 3, 101−109

Scheme 2. Resonance Structures for the 5-, 6-, and 7-Substituted 2-Methylquinolin-8-ol Derivatives

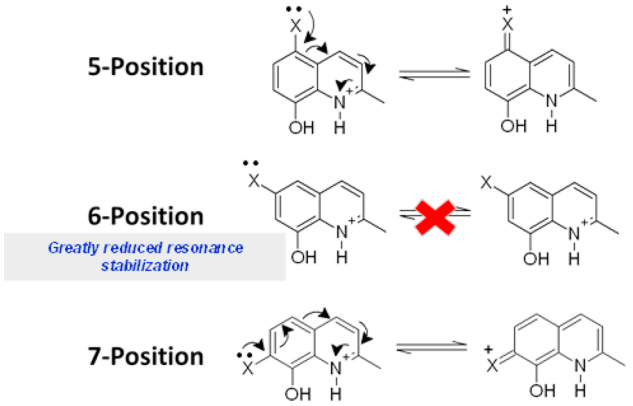

apparent trend in microsolvation of 7-substituted species tracks well with the van der Waals radii of the substituents (Table S3, Figures S7–S9). Derivatives in which the substituent in the 7-position was smaller than the methyl group in the 2-position exhibited OH–solvent binding (as was observed for the 5- and 6-substituted species). However, when the substituent in the 7-position was larger than the methyl group in the 2-position, NH–solvent binding was favored. These steric effects are visualized in Figures S7 and S8, which plot substituent van der Waals radii as a function of the relative isomer energies (i.e., OH-bound versus NH-bound). Given this clear steric effect, we postulate that 7-substituted derivatives are more easily desolvated owing to the fact that substituents in the 7-position can disrupt the extended hydrogen bonding network near the site of solvent nucleation. Further to this, nitro and methoxy groups in the 7-position are also capable of changing the microsolvation environment by forming intramolecular hydrogen bonds with the 8-hydroxy group. Thus, these species contain an intramolecular "switch", which (when engaged) enhances molecular lipophilicity.[46] Taken as a whole, these interactions weaken the ion–solvent binding energy of 7-substituted species, and this is reflected in their lower SV@CV_{min} values and enhanced cell permeabilities.

These relationships (as well as other previously identified DMS parameters,[7] Figure S2) reveal the impact of molecular structure on the DMS results (Figures 2, 3). Based upon the relative CV shifts observed, we conclude that the positioning of the substituents on the quinoline moiety affected microsolvation by providing (1) different degrees of electron donation/withdrawal from the quinoline system and (2) different levels of steric hindrance for the formation of stable ionized solute/solvent clusters. We have previously demonstrated the influence of steric hindrance in DMS, specifically in a set of quinoline molecules structurally similar to those studied here.[9] Based upon those results, we initially hypothesized that the closer the substituent on the quinoline ring to the site of charging, the weaker the microsolvation energy should be (i.e., ion–solvent binding energy for 5- < 6- < 7-substituted species). However, if the substituents are able to donate electron density to, or withdraw electron density from, the quinoline ring conjugated π-system, they would influence the molecular charge densities via resonance. As a result, ion–solvent interactions should be determined by substituent inductive resonance effects, which in turn influence ion–solvent electrostatic interactions (e.g., charge-dipole, hydrogen-bonding). For example, species with electron-withdrawing groups (e.g., –CN) should display stronger microsolvation energies because the positive partial charges at the ring NH and OH groups, the sites of solvent nucleation, will be enhanced.

From the DMS data (Figure S3, Table S1), we observe that the microsolvation energies of these species are not determined solely by the geometric distance of the substituent from the site of solvent binding (i.e., the protonated ring nitrogen and 8-hydroxyl group);[9] the electron-donating/withdrawing characteristics of the substituents in the 5-, 6-, and 7-positions are also found to play a major role in ionized solute–solvent interactions. Upon protonation of the ring nitrogen atom, resonant charge delocalization results in relatively high partial charges at the 1-, 2-, 4-, 5-, 7-, and 10-positions of the quinoline moiety. This increased positive charge of the ring system enhances the polarization of the hydroxyl group in the 8-position. When we consider the putative resonance structures of the 2-methylquinolin-8-ol derivatives (Scheme 2) and their possible roles in the observed DMS behavior, we note that substituents in the 6-position do not influence charge density of the ring system at the aforementioned positions via resonance. In this case, charge is delocalized through the π-system to a lesser extent and solvent clustering is generally strongest due to the more localized, stable charge site, compared with substitutions at 5- and 7-positions. While all 6-position substituents cluster strongly, the electron-donating substituents (e.g., methyl and methoxy) form weaker solvent clusters compared with electron-withdrawing congeners. For example, the SV@CV_{min} value and calculated ion–solvent binding energy for protonated 6-methoxy-2-methylquinolin-8-ol reveal a more weakly microsolvated species than the 6-cyano analogue (see Table S1), as expected based on electron-donating/withdrawing arguments. These differences in microsolvation energy as a function of substituent correlate strongly with the electron-donating/withdrawing properties of the functional groups (see Table S1).

We also find that the 7-substituted isomers exhibit weaker clustering interactions than do the 5-substituted isomers. Note that 7-position methoxy, methyl, and bromo substituents have >10-, 3-, and 4-fold weaker solvent binding, respectively, compared with their 5-position isomers. This difference in ion–solvent interaction strength likely arises from a moderate steric effect due to the location of the 7-substituted group proximal to the protonated ring nitrogen and 8-hydroxy group (viz., the site of solvent binding).[7,9] These structural changes may serve to destabilize the solvent shell that forms during the low-field portion of the DMS cycle. Ultimately, the 7-substituted molecules exhibit weaker microsolvation energies that may be reflective of their ability to easily desolvate/solvate as biological barriers are traversed (*vide infra*).

Addressing the Possible Importance of the Strong Local Hydrogen Bond in DMS and Physicochemical Experiments. To study drug candidates using mass spectrometry, it is necessary to probe the ionized forms (e.g., protonated 2-methylquinolin-8-ol derivatives). Nevertheless, while we are examining the solvent binding properties of the protonated species, we can extend the results obtained here to the neutral drug molecule counterparts. It is also important to note that the protonated forms of many drugs (such as these quinoline-8-ol derivatives) may play a key role in absorption given the pH of the gut environment *in vivo* (from pH ~1.7 in the stomach to ~6.5 in the intestines).[47] For the quinoline-8-ol derivatives studied here, the ring nitrogen, which is the locus of greatest

DOI: 10.1021/acscentsci.6b00297
ACS Cent. Sci. 2017, 3, 101–109

electron density, is also the site of protonation (e.g., see Figure 5).[9,48,49] This and the adjacent OH group of the quinolin-8-ol

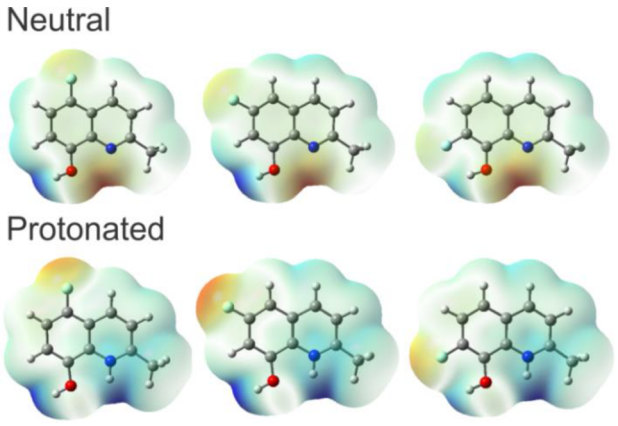

Figure 5. Charge density plots for both the neutral (top row) and protonated (bottom row) forms of three different isomers of fluoro-2-methylquinolin-8-ol. Red regions correspond to greater electron density (partial negative charge), while blue coloring maps to lesser electron density (partial positive charge).

derivatives are the principal sites of interaction for solvent molecules in both the protonated and neutral molecules. Thus, the protonated analogue is a useful example of the hydrogen bonding experienced by these drug molecules in bulk aqueous (protic) solution; intermolecular hydrogen bonding is the first step in protonation of a molecule, and these motifs have been characterized as resembling the initial stages of the proton-transfer process.[40,50,51]

We also find that the binding energy of the first solvent molecule exhibits the strongest correlation to the DMS data.[9] This accords with the hypothesis that we are probing the initial instances of the prompt solvation mechanism[52] that includes a strong local hydrogen bond formed between the drug molecule and the first solvating molecule.[53] When considering the computational accuracy of pK_a prediction, Kelly and co-workers recognized that their calculations only tracked with experimental observations when a single explicit solvent molecule was included.[53,54] While the DMS studies described herein differ from the more traditional "ion solvation" type studies conducted with mass spectrometry (i.e., where specific numbers of solvent molecules bound to an ion have been detected explicitly), some of these studies have revealed the importance of the initial ion−solvent molecule interaction.[55−57]

The work that we present here evaluates the microsolvation properties of 2-methylquinolin-8-ol derivatives with water and methanol. In future work we will investigate the effects of other volatile solvents in the DMS environment to assess the specific roles of other polar and nonpolar solvents.[58] Lastly, given the demonstrated ability of DMS to separate isomeric drug species based upon simple substitution patterns of EW and ED groups, one could envision using DMS−MS as a high-throughput platform (e.g., requiring a few minutes, not hours or days)[59] for assessing Hammett parameters experimentally, with very high degrees of both sensitivity and selectivity. While relationships between specific σ^+ constants and solvation energies have previously been postulated,[60,61] to our knowledge, this is the first time the correlation has been demonstrated experimentally.

CONCLUSIONS

In this study, we demonstrate that DMS can be used to assess the physicochemical properties of drug molecules by probing the behavior of their microsolvated forms in a robust and precise manner. These results are supported by a number of orthogonal methods, including empirically parametrized Hammett parameters and extensive computational modeling. The parallel study of DMS-determined solvent binding properties and calculated geometric and electronic structure allows us to relate the structural properties of a drug to its experimentally determined pK_a and pK_b values, and its relative cell permeability.

Overall, the correlation of DMS measurements and cell permeabilities of isomeric drugs can complement the cell-based measurements by presenting additional ways for medicinal chemists to rationalize the impact of steric and electronic effects within a chemical series. Furthermore, the SV@CV_{min} end points are very precise (<2%) and consistent across day-to-day replicate experiments, a far greater reproducibility than cell-based assays can typically achieve.[10] Hence, the combination of cell- and DMS-based methodologies could yield finer distinction between structural motifs to guide drug design. Consequently, DMS is a very promising new tool for rational drug design, where identifying and describing subtle steric and electronic interactions for a given drug structural motif facilitates the testing of structure−activity relationship hypotheses.

MATERIALS AND METHODS

Materials. Substituted 2-methylquinolin-8-ol derivatives (Scheme 1) were purchased from ACES Pharma (Princeton, NJ) and were used without further purification. HPLC grade acetonitrile and methanol were bought from Caledon Laboratory Chemicals (Georgetown, ON, Canada), and formic acid was purchased from Sigma-Aldrich (Oakville, ON, Canada). Distilled deionized water (18 MΩ) was produced in-house using a Millipore (Billerica, MA, USA) Integral 10 water purification system.

DMS−MS System. A DMS system (SCIEX, Concord, ON) was mounted on a hybrid quadrupole linear ion trap mass spectrometer (SCIEX) system in the atmospheric region between the sampling orifice and its electrospray ionization (ESI) source.[5,35] The ESI probe was maintained at a voltage of 5500 V. A constant gas flow in the DMS cell was achieved by the curtain gas flow (N_2; 30 psi, 7.1 L/min) and the primary stage vacuum pumping of the MS system. The temperature of the transport gas in the DMS cell was maintained at ∼100 °C (DMS heater setting of 150 °C). Methanol or water could be added to the curtain gas at 1.5% by a PerkinElmer 200 LC pump (Waltham, MA). In each experiment, analytes were dissolved in solution (50/50 acetonitrile/water with 0.1% formic acid) to a concentration of 100 ng/mL. Each solution was infused into the ESI source (5500 V spray voltage) at a rate of 7 μL/min.

The fundamental behavior of the DMS has been described elsewhere.[2−4,62] These experiments begin by subjecting a solution of drug molecules to ESI, producing gas-phase ions for these species. These ions are then sampled by the DMS cell: two parallel plates across which an asymmetric rf waveform (the separation voltage or SV) is applied (Figure S5). The ion's transit through the DMS cell will depend upon the amplitude of the SV (generally held at a constant value) and an additional

DOI: 10.1021/acscentsci.6b00297
ACS Cent. Sci. 2017, 3, 101−109

dc voltage (compensation voltage or CV) used to stabilize the ion's trajectory. When we purposefully add solvent vapor (e.g., water, methanol) to the DMS cell, the ions undergo dynamic clustering/declustering cycles as their trajectory and kinetic energies oscillate with the rf waveform (see Supporting Information for more detail). Consequently, the probed species undergo incipient solvation several thousand times as they transit the DMS cell. Since the collision and clustering properties of an ion also relate directly to the structural features of the ion itself, the SV/CV settings required for optimal transmission encode the statistically sampled geometries and interaction potentials of the ions with the solvent vapor molecules.[35]

Computational Methods. To identify the most stable ion−solvent cluster structures, cluster potential energy landscapes were mapped with a custom written basin-hopping (BH) algorithm.[63] Details of our implementation of the BH algorithm are reported elsewhere where we have demonstrated this methodology as an accurate means of assessing ion−solvent binding.[7,9,64,65] Convergence criteria were set to the default criteria of the Gaussian 09 suite of programs.[66] Cluster systems were modeled using the AMBER force field, with atomic partial charges calculated for the monomers with the CHelpG partition scheme[67] at the B3LYP/6-31+G(d,p) level of theory.[68,69] For each BH step, a random rotation of $-20° \leq \theta \leq 20°$ was applied about the body-fixed x, y, and z axes for each solvent molecule, and each solvent molecule was also randomly translated by -0.7 Å $\leq \eta \leq 0.7$ Å in the x, y, and z directions. BH searches explored ∼20,000 structures for clusters containing one solvent molecule. Unique isomers identified by the BH routine were optimized at the B3LYP/6-311++G(d,p) level of theory[68,69] employing the GD3 empirical dispersion correction.[70] Normal mode analyses were conducted for each isomer to ensure that it corresponded to a local minimum on the potential energy surface. In all cases, we determined that protonation occurred on the ring nitrogen. All cluster structures and *XYZ* coordinates are available in the Supporting Information. To account for basis-set superposition error in solvent binding energy calculations, counterpoise correction was employed.[71]

■ ASSOCIATED CONTENT

Supporting Information

The Supporting Information is available free of charge on the ACS Publications website at DOI: 10.1021/acscentsci.6b00297.

Figures S1−S9, Tables S1−S3, and methods (PDF)

■ AUTHOR INFORMATION

Corresponding Authors

*E-mail: john.s.janiszewski@pfizer.com.
*E-mail: scott.hopkins@uwaterloo.ca.
*E-mail: larry.campbell@sciex.com.

ORCID

Chang Liu: 0000-0003-0508-4357
W. Scott Hopkins: 0000-0003-1617-9220
J. Larry Campbell: 0000-0002-4496-7171

Notes

The authors declare no competing financial interest.

■ ACKNOWLEDGMENTS

We gratefully acknowledge high performance computing support from the SHARCNET consortium of Compute Canada. We are also grateful to Professor Terry McMahon (University of Waterloo), Dr. Tom Covey (SCIEX), and Drs. Michael Shapiro, Christopher Keefer, and George Chang (Pfizer) for helpful conversations. We thank the Natural Sciences and Engineering Research Council of Canada (NSERC) for financial support through an ENGAGE grant (EGP No. 449354-13), an ENGAGE Plus grant (EGP No. 463974-14), and a Collaborative Research and Development grant (490885). We thank the Ontario Centres of Excellence (OCE) for financial support through a Voucher for Innovation and Productivity II grant (25050).

■ REFERENCES

(1) Castleman, A.; Bowen, K. Clusters: Structure, energetics, and dynamics of intermediate states of matter. *J. Phys. Chem.* **1996**, *100* (31), 12911−12944.
(2) Krylov, E. V.; Nazarov, E. G.; Miller, R. A. Differential mobility spectrometer: Model of operation. *Int. J. Mass Spectrom.* **2007**, *266* (1−3), 76−85.
(3) Schneider, B. B.; Nazarov, E. G.; Londry, F.; Vouros, P.; Covey, T. R. Differential mobility spectrometry/mass spectrometry: History, theory, design optimization, simulations, and applications. *Mass Spectrom. Rev.* **2016**, *35*, 687−737.
(4) Shvartsburg, A. A. *Differential Ion Mobility Spectrometry: Nonlinear Ion Transport and Fundamentals of FAIMS*; CRC Press: Boca Raton, FL, 2009.
(5) Schneider, B. B.; Covey, T. R.; Coy, S. L.; Krylov, E. V.; Nazarov, E. G. Planar differential mobility spectrometer as a pre-filter for atmospheric pressure ionization mass spectrometry. *Int. J. Mass Spectrom.* **2010**, *298* (1−3), 45−54.
(6) Campbell, J. L.; Le Blanc, J. C.; Schneider, B. B. Probing electrospray ionization dynamics using differential mobility spectrometry: the curious case of 4-aminobenzoic acid. *Anal. Chem.* **2012**, *84* (18), 7857−7864.
(7) Campbell, J. L.; Zhu, M.; Hopkins, W. S. Ion−molecule clustering in differential mobility spectrometry: lessons learned from tetraalkylammonium cations and their isomers. *J. Am. Soc. Mass Spectrom.* **2014**, *25* (9), 1583−1591.
(8) Levin, D. S.; Vouros, P.; Miller, R. A.; Nazarov, E. G.; Morris, J. C. Characterization of gas-phase molecular interactions on differential mobility ion behavior utilizing an electrospray ionization-differential mobility-mass spectrometer system. *Anal. Chem.* **2006**, *78* (1), 96−106.
(9) Liu, C.; Le Blanc, J. C. Y.; Shields, J.; Janiszewski, J. S.; Ieritano, C.; Ye, G. F.; Hawes, G. F.; Hopkins, W. S.; Campbell, J. L. Using differential mobility spectrometry to measure ion solvation: an examination of the roles of solvents and ionic structures in separating quinoline-based drugs. *Analyst* **2015**, *140* (20), 6897−6903.
(10) Lintonen, T. P.; Baker, P. R.; Suoniemi, M.; Ubhi, B. K.; Koistinen, K. M.; Duchoslav, E.; Campbell, J. L.; Ekroos, K. Differential Mobility Spectrometry-Driven Shotgun Lipidomics. *Anal. Chem.* **2014**, *86* (19), 9662−9669.
(11) Hughes, J.; Rees, S.; Kalindjian, S.; Philpott, K. Principles of early drug discovery. *Br. J. Pharmacol.* **2011**, *162* (6), 1239−1249.
(12) Lipinski, C. A.; Lombardo, F.; Dominy, B. W.; Feeney, P. J. Experimental and computational approaches to estimate solubility and permeability in drug discovery and development settings. *Adv. Drug Delivery Rev.* **2012**, *64*, 4−17.
(13) Sarmento, B.; Andrade, F.; Silva, S. B. d.; Rodrigues, F.; das Neves, J.; Ferreira, D. Cell-based in vitro models for predicting drug permeability. *Expert Opin. Drug Metab. Toxicol.* **2012**, *8* (5), 607−621.
(14) Kerns, E. H. High throughput physicochemical profiling for drug discovery. *J. Pharm. Sci.* **2001**, *90* (11), 1838−1858.

DOI: 10.1021/acscentsci.6b00297
ACS Cent. Sci. 2017, 3, 101−109

(15) Chaturvedi, P. R.; Decker, C. J.; Odinecs, A. Prediction of pharmacokinetic properties using experimental approaches during early drug discovery. *Curr. Opin. Chem. Biol.* **2001**, *5* (4), 452−463.
(16) Navia, M. A.; Chaturvedi, P. R. Design principles for orally bioavailable drugs. *Drug Discovery Today* **1996**, *1* (5), 179−189.
(17) Cabot, J. M.; Fuguet, E.; Rosés, M. Internal Standard Capillary Electrophoresis as a High-Throughput Method for p K a Determination in Drug Discovery and Development. *ACS Comb. Sci.* **2014**, *16* (10), 518−525.
(18) Cai, X.; Zhang, J.; Shou, W. Z. Sample reduction strategies in discovery bioanalysis. *Bioanalysis* **2013**, *5* (13), 1691−1701.
(19) Shalaeva, M.; Kenseth, J.; Lombardo, F.; Bastin, A. Measurement of dissociation constants (pKa values) of organic compounds by multiplexed capillary electrophoresis using aqueous and cosolvent buffers. *J. Pharm. Sci.* **2008**, *97* (7), 2581−2606.
(20) Lipinski, C.; Hopkins, A. Navigating chemical space for biology and medicine. *Nature* **2004**, *432* (7019), 855−861.
(21) Volpe, D. A. Variability in Caco-2 and MDCK cell-based intestinal permeability assays. *J. Pharm. Sci.* **2008**, *97* (2), 712−725.
(22) Borchardt, R. T.; Thakker, D. R.; Warner, V. D.; Mirth, D. B.; Sane, J. N. Catechol O-methyltransferase. 8. Structure-activity relationships for inhibition by 8-hydroxyquinolines. *J. Med. Chem.* **1976**, *19* (4), 558−560.
(23) Chakrabarty, M. R.; Hanrahan, E. S.; Heindel, N. D.; Watts, G. F. Aqueous dissolution constants of 5-halo-8-hydroxyquinolines. *Anal. Chem.* **1967**, *39* (2), 238−241.
(24) Charton, M. The application of the Hammett equation to polycyclic aromatic sets. I. Quinolines and isoquinolines. *J. Org. Chem.* **1965**, *30* (10), 3341−3345.
(25) Jiang, H.; Taggart, J. E.; Zhang, X.; Benbrook, D. M.; Lind, S. E.; Ding, W.-Q. Nitroxoline (8-hydroxy-5-nitroquinoline) is more a potent anti-cancer agent than clioquinol (5-chloro-7-iodo-8-quinoline). *Cancer Lett.* **2011**, *312* (1), 11−17.
(26) Klofutar, C.; Paljk, S.; Krašovec, F.; Horvat, I. Ionization of 5-Nitro-8-hydroxyquinoline in aqueous solutions. *Microchim. Acta* **1973**, *61* (4), 559−568.
(27) Mason, S. The tautomerism of N-heteroaromatic hydroxy-compounds. Part III. Ionisation constants. *J. Chem. Soc.* **1958**, 674−685.
(28) NELDNER, K. H. The halogenated 8-hydroxyquinolines. *Int. J. Dermatol.* **1977**, *16* (4), 267−273.
(29) Paljk, Š.; Klofutar, C.; Krašovec, F.; Suhač, M. Dissociation of 8-hydroxyquinoline and its 5-chloro-and 5-nitro-derivatives in aqueous solutions. *Microchim. Acta* **1975**, *64* (4−5), 485−492.
(30) Robak, W.; Apostoluk, W.; Maciejewski, P.; Pielka, J. A.; Kwiotek, J. N. Linear Free Energy Relationship (LFER) Analysis of Dissociation Constants of 8-Hydroxyquinoline and Its Derivatives in Aqueous and Dioxane−Water Solutions. *J. Chem. Eng. Data* **2013**, *58* (6), 1470−1482.
(31) Warner, V. D.; Musto, J. D.; Sane, J. N.; Kim, K. H.; Grunewald, G. L. Quantitative structure-activity relations for 5-substituted 8-hydroxyquinolines as inhibitors of dental plaque. *J. Med. Chem.* **1977**, *20* (1), 92−96.
(32) Robak, W.; Apostoluk, W.; Ochromowicz, K. Linear solvation energy relationship (LSER) analysis of liquid−liquid distribution constants of 8-hydroxyquinoline and its derivatives. *J. Chem. Eng. Data* **2011**, *56* (11), 3971−3983.
(33) Di, L.; Whitney-Pickett, C.; Umland, J. P.; Zhang, H.; Zhang, X.; Gebhard, D. F.; Lai, Y.; Federico, J. J.; Davidson, R. E.; Smith, R. Development of a new permeability assay using low-efflux MDCKII cells. *J. Pharm. Sci.* **2011**, *100* (11), 4974−4985.
(34) Wan, H.; Holmén, A. G.; Wang, Y.; Lindberg, W.; Englund, M.; Någård, M. B.; Thompson, R. A. High-throughput screening of pKa values of pharmaceuticals by pressure-assisted capillary electrophoresis and mass spectrometry. *Rapid Commun. Mass Spectrom.* **2003**, *17* (23), 2639−2648.
(35) Schneider, B. B.; Covey, T. R.; Coy, S. L.; Krylov, E. V.; Nazarov, E. G. Chemical effects in the separation process of a differential mobility/mass spectrometer system. *Anal. Chem.* **2010**, *82* (5), 1867−1880.
(36) Artursson, P.; Palm, K.; Luthman, K. Caco-2 monolayers in experimental and theoretical predictions of drug transport. *Adv. Drug Delivery Rev.* **2001**, *46* (1), 27−43.
(37) Burton, P. S.; Conradi, R. A.; Hilgers, A. R.; Ho, N. F.; Maggiora, L. L. The relationship between peptide structure and transport across epithelial cell monolayers. *J. Controlled Release* **1992**, *19* (1), 87−97.
(38) Chikhale, E. G.; Ng, K.-Y.; Burton, P. S.; Borchardt, R. T. Hydrogen bonding potential as a determinant of the in vitro and in situ blood−brain barrier permeability of peptides. *Pharm. Res.* **1994**, *11* (3), 412−419.
(39) Wright, L. L.; Painter, G. R. Role of desolvation energy in the nonfacilitated membrane permeability of dideoxyribose analogs of thymidine. *Mol. Pharmacol.* **1992**, *41* (5), 957−962.
(40) Perrin, C. L.; Nielson, J. B. Strong" hydrogen bonds in chemistry and biology. *Annu. Rev. Phys. Chem.* **1997**, *48* (1), 511−544.
(41) Brown, H. C.; Okamoto, Y. Electrophilic substituent constants. *J. Am. Chem. Soc.* **1958**, *80* (18), 4979−4987.
(42) Hammett, L. P. Some Relations between Reaction Rates and Equilibrium Constants. *Chem. Rev.* **1935**, *17* (1), 125−136.
(43) Litwinienko, G.; DiLabio, G. A.; Mulder, P.; Korth, H.-G.; Ingold, K. Intramolecular and intermolecular hydrogen bond formation by some ortho-substituted phenols: some surprising results from an experimental and theoretical investigation. *J. Phys. Chem. A* **2009**, *113* (22), 6275−6288.
(44) Hansch, C. Quantitative structure-activity relationships and the unnamed science. *Acc. Chem. Res.* **1993**, *26* (4), 147−153.
(45) Hansch, C.; Leo, A.; Taft, R. A survey of Hammett substituent constants and resonance and field parameters. *Chem. Rev.* **1991**, *91* (2), 165−195.
(46) Goetz, G. H.; Philippe, L.; Shapiro, M. J. EPSA: A novel supercritical fluid chromatography technique enabling the design of permeable cyclic peptides. *ACS Med. Chem. Lett.* **2014**, *5* (10), 1167−1172.
(47) Charman, W. N.; Porter, C. J.; Mithani, S.; Dressman, J. B. Physicochemical and physiological mechanisms for the effects of food on drug absorption: the role of lipids and pH. *J. Pharm. Sci.* **1997**, *86* (3), 269−282.
(48) Bagno, A.; Scorrano, G. Selectivity in proton transfer, hydrogen bonding, and solvation. *Acc. Chem. Res.* **2000**, *33* (9), 609−616.
(49) Chan, B.; Del Bene, J. E.; Elguero, J.; Radom, L. On the relationship between the preferred site of hydrogen bonding and protonation. *J. Phys. Chem. A* **2005**, *109* (24), 5509−5517.
(50) Buergi, H. B.; Dunitz, J. D. From crystal statics to chemical dynamics. *Acc. Chem. Res.* **1983**, *16* (5), 153−161.
(51) Steiner, T. The hydrogen bond in the solid state. *Angew. Chem., Int. Ed.* **2002**, *41* (1), 48−76.
(52) Ladanyi, B. M.; Stratt, R. M. Short-time dynamics of solvation: Relationship between polar and nonpolar solvation. *J. Phys. Chem.* **1996**, *100* (4), 1266−1282.
(53) Kelly, C. P.; Cramer, C. J.; Truhlar, D. G. Adding explicit solvent molecules to continuum solvent calculations for the calculation of aqueous acid dissociation constants. *J. Phys. Chem. A* **2006**, *110* (7), 2493−2499.
(54) Adam, K. R. New density functional and atoms in molecules method of computing relative p K a values in solution. *J. Phys. Chem. A* **2002**, *106* (49), 11963−11972.
(55) Bohme, D. K.; Mackay, G. I. Bridging the gap between the gas phase and solution: transition in the kinetics of nucleophilic displacement reactions. *J. Am. Chem. Soc.* **1981**, *103* (4), 978−979.
(56) Chang, T. M.; Prell, J. S.; Warrick, E. R.; Williams, E. R. Where's the charge? Protonation sites in gaseous ions change with hydration. *J. Am. Chem. Soc.* **2012**, *134* (38), 15805−15813.
(57) Gao, B.; Wyttenbach, T.; Bowers, M. T. Protonated arginine and protonated lysine: hydration and its effect on the stability of salt-bridge structures. *J. Phys. Chem. B* **2009**, *113* (29), 9995−10000.

DOI: 10.1021/acscentsci.6b00297
ACS Cent. Sci. 2017, 3, 101−109

(58) Oehlke, A.; Auer, A. A.; Schreiter, K.; Hofmann, K.; Riedel, F.; Spange, S. Electrophilic Substituent Constant σ+ of Electron Donor Substituents in Nonpolar Media. *J. Org. Chem.* **2009**, *74* (9), 3316−3322.
(59) Portal, C. F.; Bradley, M. High-Throughput Physical Organic Chemistry Hammett Parameter Evaluation. *Anal. Chem.* **2006**, *78* (14), 4931−4937.
(60) DiLabio, G. A.; Ingold, K. Solvolysis of para-substituted cumyl chlorides. Brown and Okamoto's electrophilic substituent constants revisited using continuum solvent models. *J. Org. Chem.* **2004**, *69* (5), 1620−1624.
(61) Oyama, K.; Tidwell, T. T. Cyclopropyl substituent effects on acid-catalyzed hydration of alkenes. Correlation by. sigma.+ parameters. *J. Am. Chem. Soc.* **1976**, *98* (4), 947−951.
(62) Purves, R. W.; Guevremont, R. Electrospray ionization high-field asymmetric waveform ion mobility spectrometry-mass spectrometry. *Anal. Chem.* **1999**, *71* (13), 2346−2357.
(63) Wales, D. J.; Doye, J. P. K. Global optimization by basin-hopping and the lowest energy structures of Lennard-Jones clusters containing up to 110 atoms. *J. Phys. Chem. A* **1997**, *101* (28), 5111−5116.
(64) Hopkins, W. S.; Marta, R. A.; McMahon, T. B. Proton-Bound 3-Cyanophenylalanine Trimethylamine Clusters: Isomer-Specific Fragmentation Pathways and Evidence of Gas-Phase Zwitterions. *J. Phys. Chem. A* **2013**, *117* (41), 10714−10718.
(65) Campbell, J. L.; Yang, A. M.-C.; Melo, L. R.; Hopkins, W. S. Studying Gas-Phase Interconversion of Tautomers Using Differential Mobility Spectrometry. *J. Am. Soc. Mass Spectrom.* **2016**, *27*, 1277−1284.
(66) Frisch, M. J.; Trucks, G. W.; Schlegel, H. B.; Scuseria, G. E.; Robb, M. A.; Cheeseman, J. R.; Scalmani, G.; Barone, V.; Mennucci, B.; Petersson, G. A.; Nakatsuji, H.; Caricato, M.; Li, X.; Hratchian, H. P.; Izmaylov, A. F.; Bloino, J.; Zheng, G.; Sonnenberg, J. L.; Hada, M.; Ehara, M.; Toyota, K.; Fukuda, R.; Hasegawa, J.; Ishida, M.; Nakajima, T.; Honda, Y.; Kitao, O.; Nakai, H.; Vreven, T.; Montgomery, J. A., Jr.; Peralta, J. E.; Ogliaro, F.; Bearpark, M.; Heyd, J. J.; Brothers, E.; Kudin, K. N.; Staroverov, V. N.; Kobayashi, R.; Normand, J.; Raghavachari, K.; Rendell, A.; Burant, J. C.; Iyengar, S. S.; Tomasi, J.; Cossi, M.; Rega, N.; Millam, N. J.; Klene, M.; Knox, J. E.; Cross, J. B.; Bakken, V.; Adamo, C.; Jaramillo, J.; Gomperts, R.; Stratmann, R. E.; Yazyev, O.; Austin, A. J.; Cammi, R.; Pomelli, C.; Ochterski, J. W.; Martin, R. L.; Morokuma, K.; Zakrzewski, V. G.; Voth, G. A.; Salvador, P.; Dannenberg, J. J.; Dapprich, S.; Daniels, A. D.; Farkas, Ö.; Foresman, J. B.; Ortiz, J. V.; Cioslowski, J.; Fox, D. J. *Gaussian 09, revision A.1*; Gaussian, Inc.: Wallingford, CT, 2009.
(67) Wiberg, K. B.; Rablen, P. R. Comparison of atomic charges derived via different procedures. *J. Comput. Chem.* **1993**, *14* (12), 1504−1518.
(68) Becke, A. D. Density-functional thermochemistry 0.3. The role of exact exchange. *J. Chem. Phys.* **1993**, *98* (7), 5648−5652.
(69) Lee, C. T.; Yang, W. T.; Parr, R. G. Development of the colle-salvetti correlation-energy formula into a functional of the electron-density. *Phys. Rev. B: Condens. Matter Mater. Phys.* **1988**, *37* (2), 785−789.
(70) Grimme, S.; Antony, J.; Ehrlich, S.; Krieg, H. A consistent and accurate ab initio parametrization of density functional dispersion correction (DFT-D) for the 94 elements H-Pu. *J. Chem. Phys.* **2010**, *132* (15), 154104.
(71) Simon, S.; Duran, M.; Dannenberg, J. J. How does basis set superposition error change the potential surfaces for hydrogen bonded dimers? *J. Chem. Phys.* **1996**, *105* (24), 11024−11031.

DOI: 10.1021/acscentsci.6b00297
ACS Cent. Sci. 2017, 3, 101−109